

# Accepted Manuscript

A novel plectin/integrin-targeted bispecific molecular probe for magnetic resonance/near-infrared imaging of pancreatic cancer

Qian Wang, Hao Yan, Yushen Jin, Zihua Wang, Wenhui Huang, Jia Qiu, Feiyu Kang, Kun Wang, Xinming Zhao, Jie Tian



PII: S0142-9612(18)30608-2

DOI: [10.1016/j.biomaterials.2018.08.048](https://doi.org/10.1016/j.biomaterials.2018.08.048)

Reference: JBMT 18854

To appear in: *Biomaterials*

Received Date: 13 April 2018

Revised Date: 16 August 2018

Accepted Date: 20 August 2018

Please cite this article as: Wang Q, Yan H, Jin Y, Wang Z, Huang W, Qiu J, Kang F, Wang K, Zhao X, Tian J, A novel plectin/integrin-targeted bispecific molecular probe for magnetic resonance/near-infrared imaging of pancreatic cancer, *Biomaterials* (2018), doi: 10.1016/j.biomaterials.2018.08.048.

This is a PDF file of an unedited manuscript that has been accepted for publication. As a service to our customers we are providing this early version of the manuscript. The manuscript will undergo copyediting, typesetting, and review of the resulting proof before it is published in its final form. Please note that during the production process errors may be discovered which could affect the content, and all legal disclaimers that apply to the journal pertain.

A Novel Plectin/Integrin-targeted Bispecific Molecular Probe for  
Magnetic Resonance/Near-infrared Imaging of Pancreatic Cancer

Short title: Novel probe for early pancreatic cancer diagnosis

Qian Wang<sup>a,b,#</sup>, Hao Yan<sup>b,c,#</sup>, Yushen Jin<sup>b</sup>, Zihua Wang<sup>d</sup>, Wenhui Huang<sup>b</sup>, Jia Qiu<sup>b</sup>,  
Feiyu Kang<sup>c</sup>, Kun Wang<sup>b,\*</sup>, Xinming Zhao<sup>a,\*</sup>, Jie Tian<sup>b,\*</sup>

# These authors contributed equally to this work

\* Corresponding authors

<sup>a</sup> Department of imaging diagnosis National Cancer Center/National Clinical Research Center for Cancer/Cancer Hospital, Chinese Academy of Medical Sciences and Peking Union Medical College, Beijing, 100021, China

<sup>b</sup> CAS Key Laboratory of Molecular Imaging, Institute of Automation Chinese Academy of Sciences, Beijing 100190, China

<sup>c</sup> School of Materials Science and Engineering, Graduate School at Shenzhen, Tsinghua University, Beijing 100190, China

<sup>d</sup> Key Laboratory of Colloid Interface and Chemical Thermodynamics, Institute of Chemistry Chinese Academy of Sciences, Beijing 100190, China

\*Corresponding author:

E-mail: xinmingzh2017@yeah.net

E-mail: kun.wang@ia.ac.cn & jie.tian@ia.ac.cn

## Abstract

Pancreatic ductal adenocarcinoma (PDAC) is one of the deadliest human malignancies with poor patient outcomes often resulting from delayed diagnosis. Therefore, early diagnosis can lead to a better prognosis and improved outcomes. In this study, we have developed a novel conjugate complex of plectin/integrin-targeted bispecific molecular probe, termed Gd-Cy7-PTP/RGD, to be used for magnetic resonance/near-infrared imaging (MRI/NIRF) of pancreatic cancer *in vivo*. This bispecific molecular probe comprises four parts: Gd(III) for MRI, cyanine 7 (Cy7) for NIRF, the peptide PTP for binding to plectin-1 specifically overexpressed on the surface of PDAC cells, and the peptide RGD for targeting integrin widely expressed on pancreatic duct epithelial cells and angiogenesis. Remarkably, the combination of PTP and RGD greatly increased the targeting efficiency *in vitro* and *in vivo* compared to that of either single peptide. Moreover, such bispecific molecular probes target pancreatic neoplasms and angiogenesis simultaneously, producing a “multi-level” targeting effect confirmed by immunofluorescence testing *in vitro* and *in vivo*. Under the guidance of MRI/NIRF dual-modality imaging, NIRF-guided delineation of surgical margins during operations was successfully achieved in orthotopic pancreatic cancer. This study promotes further exploration of bispecific molecular probes for clinical application.

**Keywords:** Bispecific peptides, Early diagnosis, Molecular imaging, Pancreatic cancer, Theranostics

## 1. Introduction

Pancreatic cancer (PC) is among the most lethal cancers, with an overall 5-year survival rate of approximately 7% [1]. One important reason for the poor survival is that the majority (over 85%) of patients are diagnosed with advanced diseases and have poor prognoses [2, 3]. However, successful early-stage pancreatic ductal adenocarcinoma (PDAC) and resection of the incipient lesions can increase the 4-year

survival rate of PC up to 78% [4, 5]. Therefore, early diagnosis leads to better prognoses and outcomes for patients. Molecular probes combined with current imaging systems can bind and detect disease-specific molecules present several years before the appearance of symptoms [6], and thus may enable diagnosis of incipient disease among individuals with no obvious symptoms [7]. There are two key components to molecular imaging constructs, including a highly specific ligand for active targeting and a contrast agent for visualization.

At present, several biomarkers have been successfully explored, applied to targeting of pancreatic cancer, and have truly enhanced the prognosis of the disease in preclinical research. These biomarkers include mesothelin [8], urokinase plasminogen activator (uPA) [9], insulin-like growth factor I receptor (IGF-1R) [10], mucin 1 [11], vascular endothelial growth factor receptor 2 (VEGFR2) [12], zinc transporter 4 (ZIP4) [13], and carbohydrate antigen 19-9 (CA19-9) [14]. However, pancreatic cancer is genetically complex and heterogeneous, with even a single tumor mass from a given patient containing up to 63 genetic alterations and 12 core signal pathway abnormalities [15], to say nothing of the heterogeneity of tumor biomarker expression among different cancer patients [2]. Thus, effective targeting will probably need to attack several targets simultaneously through combined regimens [16].

Plectin, a traditional cytoskeleton scaffolding protein, has recently gained considerable attention as a target for PDAC detection *in vivo* [17] and in clinical trials [18] because of its exclusively aberrant mislocalization on the surface of the pancreatic cancer epithelium [19]. Integrins, a family of cellular adhesion molecules involved in tumorigenesis and tumor progression [20], have been widely shown efficient targets and biomarkers for the detection of PDAC [21, 22]. Interestingly, there is a close relationship between plectin and integrins. Integrin  $\beta 4$  (ITGB4) has proved indispensable to plectin mislocalization in PDAC [19]. Plectin-1 and ITGB4 directly interact with one another and play an important role in PDAC proliferation and migration [19]. Moreover, plectin and integrin are exclusively overexpressed in different areas of PDAC, plectin in the ductal epithelial cells and integrin in PDAC cells and angiogenesis. Therefore, combining plectin and integrin as targeting

biomarkers may amplify targeting efficiency and produce the “multi-level” targeting effect as targeting neoplastic parenchyma and tumor vasculature in molecular imaging of PDAC, which has not yet been reported, to our knowledge.

Additionally, PDAC is characterized by the presence of a dense desmoplastic stroma, hypovascular and hypoperfused tumor vessels, and increased interstitial fluid pressure within the tumor that render most nanoparticle-based delivery ineffective [23]. A recent analysis of literature from the past 10 years indicated that less than 0.4% of administered nanoparticles are delivered to solid tumors in PDAC [24, 25], well below the 0.7% (median) average of all types of cancer [26]. Additionally, considering the long-term safety *in vivo* and clinical translational prospects, small molecular probes may be more suitable for imaging of PDAC. Molecular imaging also requires the use of specialized contrast agents to ensure optimal tissue contrast. Among the various imaging modalities, MRI is widely used in clinics and provides independent imaging with high soft-tissue contrast [27]. NIRF imaging can reveal real-time pharmacokinetics and biodistribution in the whole body with high sensitivity and specificity, but it suffers from low spatial resolution and poor tissue penetration [28]. Therefore, the combination of MRI and NIRF not only integrates their individual advantages and overcomes their intrinsic limitations, but also provides accurate and comprehensive diagnostic information to guide surgery. However, the synthesis and application of bispecific molecular probes to integrate plectin/integrin-targeted peptides and MRI/NIRF molecular contrast agents are still formidable challenges.

In this study, a novel bispecific molecular probe, Gd-Cy7-PTP/RGD, consisting of two peptides (PTP/RGD) for targeting plectin/integrin was developed and applied to MRI/NIRF dual-modality imaging and surgical navigation, as shown in Fig. 1. Plectin-targeted polypeptide (PTP, short for KTLLPTP) exclusively targets pancreatic cancer cells. The integrin-targeting polypeptide (RGD) widely targets the whole pancreatic neoplasm and angiogenesis. After synthesis, the bispecific molecular probe maintained both excellent targeting properties and imaging characteristics. The combination of PTP and RGD peptides greatly increased the binding efficiency of the probes to their targets and achieved the “multi-level” targeting effect *in vitro* and *in*

*vivo*. Furthermore, the bispecific molecular probe facilitated dual-modality imaging: whole-body tumor localization using MRI as well as high-sensitivity, high-specificity, and real-time imaging using NIR fluorescence imaging. Under the guidance of preoperative diagnostic information, NIRF-guided delineation of surgical margins during resection of pancreatic cancer was successfully achieved in an orthotopic pancreatic cancer model. Our work not only demonstrated the advantages of bispecific targeting in PDAC but also encourages further exploration of such molecular probes for future clinical applications.

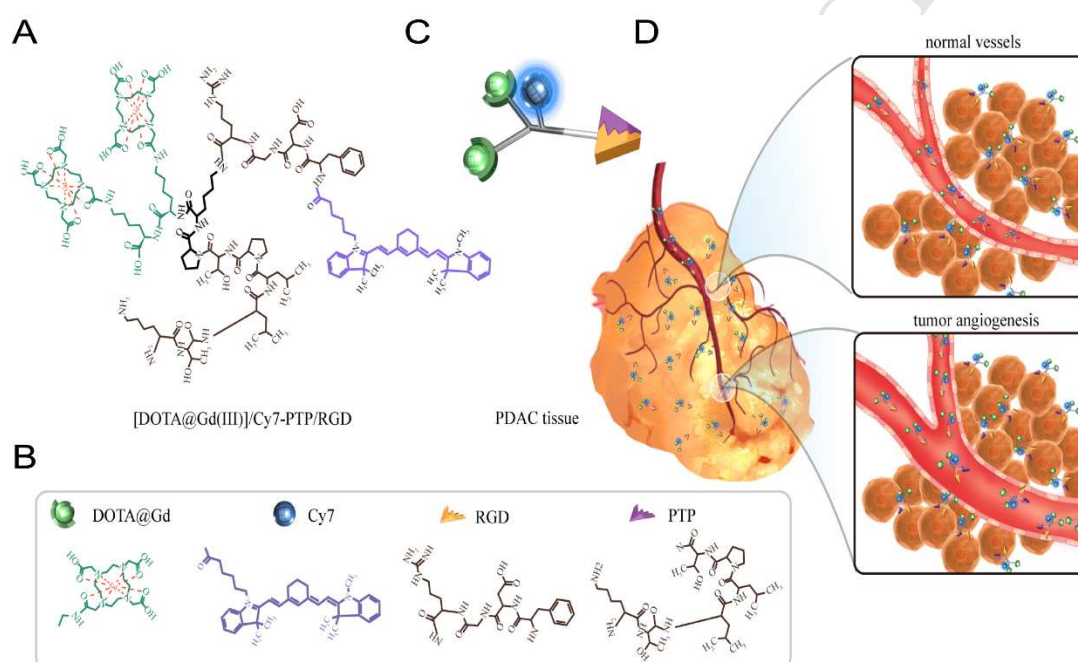


**Fig. 1. Schematic illustration of the bispecific probe targeting PDAC.** (A) Molecular structural formula of Gd-Cy7-PTP/RGD. (B) Schematic illustration of the preparation of Gd, Cy7, PTP, and RGD. (C) Clear diagram of Gd-Cy7-PTP/RGD. (D) Schematic illustration of Gd-Cy7-PTP/RGD with bispecific targeting of plectin/integrin in PDAC.

## 2. Materials and methods

### 2.1 Synthesis and Characterization of Gd-Cy7-PTP/RGD

1, 4, 7, 10-tetraazacyclododecane-1,4,7,10-tetraacetic acid (DOTA),  $\text{GdCl}_3 \cdot 6\text{H}_2\text{O}$  and Cyanine7 ester (Cy7-NHS) were purchased from Aladdin Chemical Co, Ltd. 3-(4, 5-Dimethylthiazol-2-yl)-2, 5-diphenyl tetrazolium bromide (MTT), fluorescein isothiocyanate (FITC), Alexa Fluor 488/647 (AF488/AF647), and (40,6-diamidino-2-phenylindol) (DAPI) were purchased from Sigma-Aldrich.

Bispecific probe preparation based on the previous reports [29-30]. Polypeptides were

synthesized by solid-phase methods using a standard Fmoc-Chemistry. This process was repeated from C-terminal to N-terminal as follows: Fmoc-Lys (Dde)-Fmoc-Lys (Alloc)-Fmoc-Pro-Fmoc-Thr (tBu)-Fmoc-Pro-Fmoc-Leu-Fmoc-Leu-Fmoc-Thr (tBu)-Fmoc-Lys (Boc), which was simplified as KTLLPTPKRGDFKK. After each reaction cycle, the resin was thoroughly washed for the subsequent preparation. Cy7-NHS ester (5 mg) was conjugated to the N-terminal of side chain of bi-peptides (15 mg) on the resin in the presence of coupling agents (HATU: DIEA, 3:10). After [DOTA (tBu)<sub>3</sub>-ester] was coupled to the amine of Lys (Dde) by hydrazine hydrate selective deprotection Dde on peptide. The peptide and other protection of the amino acid side chains were cleaved by TFA (95% v/v), H<sub>2</sub>O (2.5% v/v) and TIPS (2.5% v/v) for 3 h. A crude precursor as KTLLPTPK(RGDF-Cy7)-K(DOTA)-K(DOTA) was harvested through centrifugation and washed to yield (16.45 mg, 34.27%). 5.0 mg Gd chloride hexahydrate (13.45  $\mu$ mol) was added in the precursor mixture (1.0 mL), stirred overnight at room temperature. The mixture solution was purified using a dialysis bag (molecular cut off, 1KDa) and then was condensed and lyophilized in the dark. The robust product as KTLLPTPK (RGDF-Cy7) K(DOTA@Gd)-K(DOTA@Gd) was obtained (13.94 mg, 28.46%), simplified as Gd-Cy7-PTP/RGD.

The final product and its precursor were characterized by high-performance liquid chromatography (HPLC) and mass spectrometry (MS) and described in the supporting information. UV spectrophotometer (UV-2450; Shimadzu) was used to measure optical characteristic and serum stability. Longitudinal relaxation ( $T_1$ ) of the probe was measured at varying Gd(III) concentrations using a 7.0 T MR (Bruker BioSpec 70/20, Germany) scanner.

## 2.2 Cellular culture

Human pancreatic cancer cells (Aspc1, Panc1, Bxpc3, SW1990, Capan2, T3M4), human pancreatic ductal epithelial cells (HPDE6-C7), human umbilical endothelial vein cells (HUVEC), mouse fibroblast cells (L929) were gifted by National key laboratory of tumor hospital of Chinese academy of medical sciences. They were cultured in high-glucose DMEM and RPMI medium and supplemented with 10% (v/v) fetal bovine serum FBS, 1% penicillin and 1% streptomycin. The cells were maintained in a humidified atmosphere of 5% CO<sub>2</sub> at 37 °C.

## 2.3 Western blot analysis

Six pancreatic cancer cells were lysed in 1×PBS, 1% Nonidet P-40, 2  $\mu$ g/mL Aprotinin, 2  $\mu$ g/mL Leupeptin, and 50  $\mu$ g/mL phenylmethylsulfonyl fluoride (PMSF). Cell lysates were then centrifuged at 12,000  $\times$ g at 4°C for 30 min. The total proteins were extracted from the supernatants. Proteins were separated through sodium dodecyl sulfate polyacrylamide gel electrophoresis SDS-PAGE (10% resolving gel) and electroblotted onto a polyvinylidene fluoride (PVDF) membrane. The membrane was blocked with 1× PBST buffer for 30 min, incubated with the indicated primary antibodies and anti-mouse or anti-rabbit secondary antibodies conjugated with horseradish peroxidase. Chemiluminescence signals were detected using *ImageQuant* LAS 4000 (GE Healthcare Life Sciences).

## 2.4 Cellular toxicity

*In vitro* cytotoxicity was measured using a standard MTT assay kit. Three kinds of cells were seeded in 96-well plates at a density of 10<sup>4</sup> cells/100  $\mu$ L culture per well for 24 h. Thereafter, the

culture medium was replaced by equal volumes of media containing six different concentrations of Gd-Cy7-PTP/RGD probe (0–200  $\mu\text{g/mL}$ ) and cells were incubated. After 24 hours, the cells were washed with PBS three times and then mixed with 100  $\mu\text{L}$  of media and MTS (20  $\mu\text{L}$ ) were added to each well. Cell viability was assessed by measuring optical absorbance at 490 nm, using a Synergy HT microplate reader (BioTek, USA).

### 2.5 *In vitro* binding affinity assays of Bi-peptides

According to previous report [31],  $10^5$  cells including human pancreatic cancer panc1 cells, mouse L929 fibroblast cells, human HUVEC cells and human normal pancreatic duct epithelial cells as HPDE6-C7 cells, were seeded into a confocal capsule for 24 h at  $37^\circ\text{C}$  in  $\text{CO}_2$  incubators and then fixed with paraformaldehyde. After PBS washing three times, cells were incubated with PTP labeled AF488 and RGD labeled AF647 (peptide/dye: 1/1.5) at room temperature for 4 h in the dark, respectively. Thereafter, the cell nucleus was stained with DAPI for 5 min. For blocking studies, cells were preincubated with 1 mL (20  $\mu\text{g/mL}$ ) anti-plectin-1 McAb (monoclonal antibody) and anti-ITGB4 McAb for 2 h for blocking. Furthermore, HPDE6-C7 cells, as negative control, were incubated directly with bi-peptides labeled FITC. The cells were observed in PE fluorescence confocal microscope (PE ultraview) and imaged with a ZEN 2012. Co-localization of bi-peptides on the Panc1 cells was analyzed using *Image J* 2X. And overlap scatter plots and Mander's coefficient for overlap were analyzed by *Image proplus6.0* software.

Panc1 and HPDE6-C7 cells were plated into four 6-well plates at a density of  $10^4$  cells per well and incubated in culture medium for 24 h. Thereafter, culture media were replaced with fresh media containing six FITC concentrations (0–2.0  $\mu\text{g/mL}$ ) of bi-peptides labeled FITC and incubated with cells for 4 h. After PBS washing three times, the cells were digested with EDTA and centrifuged at  $100 \times g$  for 3 min [32]. Samples were assessed to test using *BD Accuri C6* and analyzed by *Flow Jo* 7.6.

Subsequently, Enzyme linked immunosorbent assay was performed. Panc1 and HPDE6-C7 cell homogenates were prepared by two times freeze-thaw cycles in ice-cold  $1 \times \text{PBS}$ . Then the homogenates were centrifuged for 5 minutes at 5000g. Remove the supernate and assay immediately. The following procedure was performed in accordance with the protocol provided by Wuhan ELIab Science Co. Ltd's ELISA kits with little change. Firstly, 100  $\mu\text{L}$  cell homogenates or bovine serum albumin (BSA) were added into per well of 96-well plate. After incubation for 2 hours at  $37^\circ\text{C}$ , Human Plectin-1 or ITGB4 first antibody, the corresponding IgG and Bi-peptide were added into the corresponding wells and incubated at  $37^\circ\text{C}$  for 1 hour. Secondly, remove the liquid of each well then add 100  $\mu\text{L}$  of detection reagent A which provided by the ELISA kit. Then detection reagent B, substrate solution and stop solution were added successively. At last, determine the optical density of each well at once, using a microplate reader set to 450 nm.

### 2.6 *Animals and Tumor model*

All experiments involving animals were performed in accordance with the guidelines of the Animal Ethics Committee of the Chinese Academy of Medical Sciences tumor hospital [NCC2016A002]. 6-weeks-old female BALB/C nude mice purchased from Beijing Vital River Laboratory Animal Technology Co. Ltd (China). Mice were injected with Panc1 cells (0.2 mL in H-DMEM culture medium without FBS,  $\approx 1 \times 10^6$ ) and tumor models were subcutaneously and orthotopically established. The mice were used when their tumor volumes approached 80–100

mm<sup>3</sup>.

## 2.7 *In vivo confocal fluorescence laser microscopy (CFL) of Bi-peptides*

CFL imaging was performed as described [33] using the Cellvizio488 and 660 laser scanning units for non-specific FITC imaging as control, and RGD labeled AF488 and PTP labeled AF647 for specific imaging. Mice bearing Panc1 tumor were injected with FITC (100  $\mu$ L, 1 mg/mL) via tail vein for pancreatic tumor and tumor vessel for *in vivo* morphological analysis. For specific targeting of bi-peptides probe, mice were injected via tail vein with bi-peptides labeled AF647 (100  $\mu$ L, 1 mg/mL) for specific distribution to tumor. For further investigation for bi-peptides targeting mechanism, mice were injected via tail vein with RGD labeled AF488 and PTP labeled AF647 (100  $\mu$ L, 1 mg/mL), respectively for the distribution of RGD and PTP targeting to tumor. Tumor masses were excised rapidly and fixed in tissue freezing medium with OCT gel. The frozen sections were stained with DAPI (100  $\mu$ g/mL) for 5 min. The slices were visualized by 3D HISTECH software [34].

## 2.8 *In vivo optical and MR imaging of Gd-Cy7-PTP/RGD*

For *in vivo* optical imaging, BALB/c mice were intravenously injected with Gd-Cy7-PTP/RGD, (0.15 mL of a 0.5 mg/mL solution for each mouse), one group injected with free Cy7 as non-specific control. For blocking studies, mouse anti-human plectin-1 McAb and anti-human ITGB4 McAb was pre-injected 4 h in advance, respectively. And fluorescent signals were detected at various time points. Fluorescence intensity was presented as the average radiant efficiency in the unit of [p/sec/cm<sup>2</sup>/sr]/ [mW/cm<sup>2</sup>]. Fluorescence intensity of the *ex vivo* tumor and main organs at different time was measured and tumor background ratio (TBR) at different time was calculated.

For *in vivo* MR imaging, BALB/c mice were intravenously injected at a dose of 0.03 mmol Gd/kg (100  $\mu$ L), respectively. The same protocol was performed as Gd control.  $T_1$ -weighted images were acquired at 4 h and 24 h post injection, respectively.  $T_1$ -weighted images were acquired with a  $T_1$ -TSE sequence using the mouse body volume coil. The sequences used were TSE  $T_1$  axial view (parameters: FOV 40 mm, slice thickness 3.0 mm, TR 232 ms, TE 30 ms, four averages). And SNR measurement according to:  $SNR = S - S_b / SD$ , SNR: signal noise ratio,  $S$ : Signal of objective,  $S_b$ : Singal of background,  $SD$ : image niose. The standard deviation of the more homogeneous background area is meaning image noise.

Then tumors and main organs were dissected out and homogenized with concentrated nitric acid (1.0 mL, 70%, EMD, Gibbstown, NJ, USA). The samples were liquefied for 4 days and the solutions were centrifuged at 15,000 rpm for 8 minutes. The supernatant liquor was diluted with deionized water. Gd (III) concentration was measured by ICP-OES. Gd (III) content was determined as the percentage of injected dose per gram of organ/tissues (% ID/g).

## 2.9 *Optical imaging-guided surgery of Gd-Cy7-PTP/RGD*

For optical imaging-guided surgery, mice bearing orthotopic Panc1 xenografts were injected i.v. with 0.5 nmol Gd-Cy7-PTP/RGD. Mice were anesthetized and optical imaging was performed at 4 h p.i to localize the nodules and then were sacrificed to thoroughly resect tumor nodules. NIRF-guiding system navigated tumor excision. For further confirmation of orthotopic lesions in the pancreas, surgically excised tumor lesions were fixed in 5% buffered formalin and embedded

in paraffin, cut into sections, and subjected to hematoxylin and eosin (H&E) staining. And also, the excised tumor was made into frozen sections for NIRF imaging. The frozen sections (thickness, 20  $\mu\text{m}$ ) were exposed to bright field and NIR field (800 nm) using a Leica CM1950 machine.

**Statistical analysis:** Quantitative data are expressed as means  $\pm$  SD. Means were compared using one-way analysis of variance (ANOVA) and Student's *t* test. *P* values  $<0.05$  were considered statistically significant.

### 3. Results and Discussion

#### 3.1 Synthesis and characterization of Gd-Cy7-PTP/RGD

Gd-Cy7-PTP/RGD was synthesized by a solid-phase reaction (Fig. S1). Firstly, the synthesized precursor prior to Gd(III) chelation was confirmed by analytical HPLC and MS analyses and had molecular weight 2933.18 and purity 99.33% (Fig. S2). While the end product after chelation had molecular weight 3676.94 and purity 95.38% (Fig. S3), proving successful chelation, which is clearly shown in the 3D model in Fig. S4.

Bispecific probe labeled with Cy7 NHS ester yielded a characteristic peak at 748 nm, similar to the absorption waveform of free Cy7 (Fig. 2A), showing successful labeling. UV absorption exhibited a negligible change after conjugation with Cy7, implying that the Cy7 NHS ester linkage to the side chain of lysine was effective and stable with a 1:1 molar ratio after solid-phase synthesis. Fluorescence intensity and UV absorption in the 50% FBS/PBS mixture only slightly decreased within 48 h, as shown in Fig. 2B. Fig. S5A and B show that there were only slight declines of either fluorescence intensity or UV absorption at varying time points.

Additionally, the fluorescence intensity of Gd-Cy7-PTP/RGD changed with Cy7 concentration, as shown in Fig. 2C, and the  $T_1$  relaxivity changed with Gd(III) concentration, as shown in Fig. 2D. Fluorescence was positively correlated with Cy7 concentration, but sharply dropped when Cy7 concentration reached to 20.4  $\mu\text{g/mL}$ , suggesting that aggregation of Gd-Cy7-PTP/RGD has a fluorescence-quenching effect similar to that of free Cy7. Besides,  $T_1$  relaxivity (longitudinal relaxation ratio) at different Gd(III) concentrations was examined, and typical  $T_1$ -weighted MR images at 7.0 *T* are shown in Fig. 2D. The  $T_1$  relaxivity of Gd-Cy7-PTP/RGD was 6.88  $\text{mM}^{-1}\text{s}^{-1}$  per molecule and exceeded 3.57  $\text{mM}^{-1}\text{s}^{-1}$  per molecule of Gd at room temperature.

This suggests that the bispecific probe possessed more distinguished  $T_1$  relaxivity than did Gd.

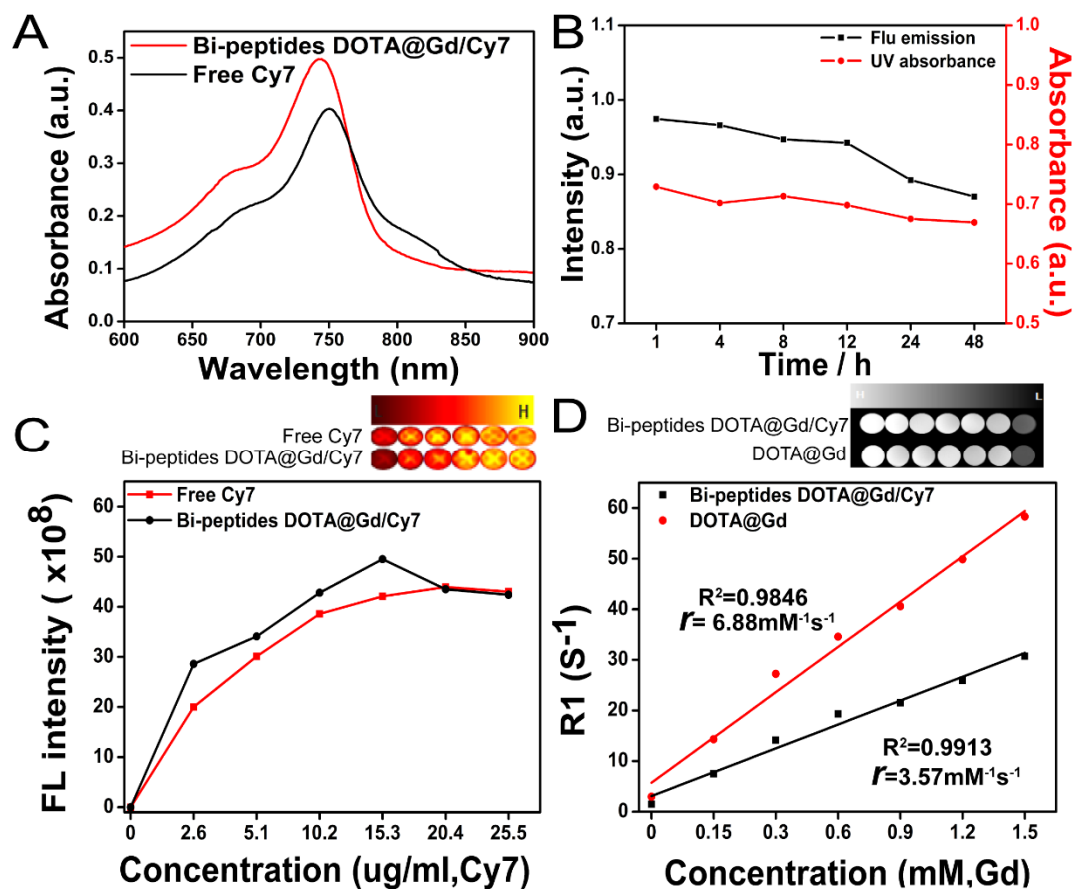


**Fig. 2. Characterization of bispecific probe.** (A) UV absorption characterization of Gd-Cy7-PTP/RGD. (B) Fluorescence spectrum of probe at 1, 4, 8, 12, 24, and 48 h. (C) Fluorescence intensity changes with varying Cy7 concentrations. (D)  $T_1$ -weighted MR images of Gd-Cy7-PTP/RGD and Gd at varying Gd(III) concentrations.

Hence, these results demonstrated that the fluorescence performances and UV properties were unaffected by specific, conjugated targeting elements; meanwhile, the  $T_1$  relaxivity compared with that of Gd alone was greatly improved, consistently with previous reports [29].

### 3.2 Plectin-1/ ITGB4 expression in human pancreatic cancer cell lines

The expression of both plectin-1 and ITGB4 was evaluated in human pancreatic cancer cell lines, such as Aspc1, Bxpc3, Panc1, SW1990, Capan2, and T3M4. Actin (muscle protein) and GAPDH (glyceraldehyde-3-phosphate dehydrogenase) were used as internal controls for normalization of relative abundance after western blotting.

Plectin-1 had high expression across the cell lines. ITGB4 was overexpressed in most cell lines. As shown in Fig. 3, both plectin-1 and ITGB4 were overexpressed in Panc1 cells; thus, these cells were used in the following *in vitro* and *in vivo* experiments. Theoretically, this also meant that the bispecific probe (PTP/RGD) should have high binding affinity to Panc1 cells *in vitro* or *in vivo*.

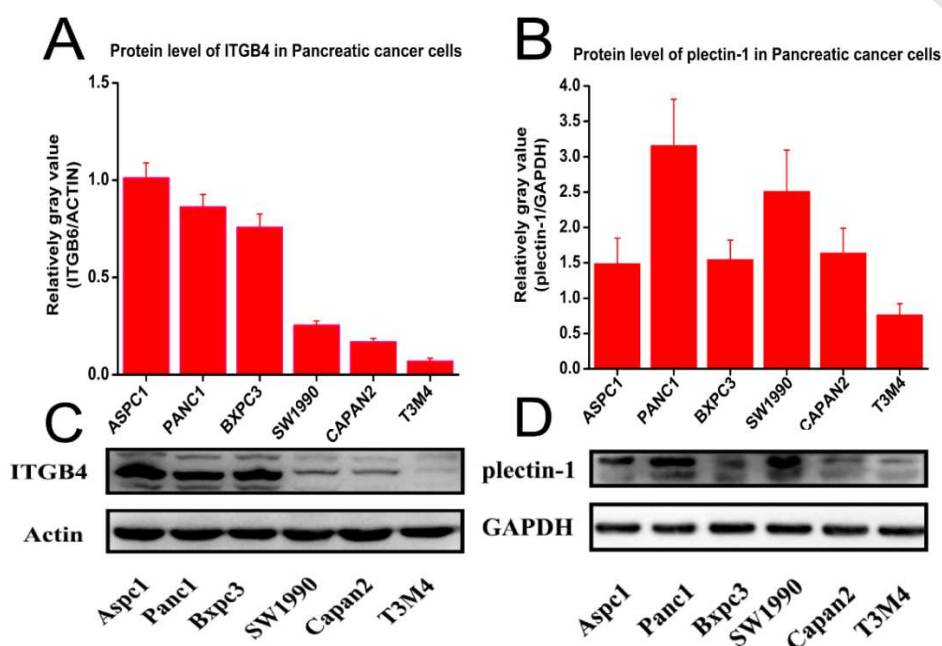


**Fig. 3. Western blotting for ITGB4 and plectin-1 expression in human pancreatic cancer cell lines.** (A) Relative abundance of ITGB4. (B) Relative abundance of plectin-1. (C) ITGB4 was universally highly expressed in pancreatic cancer cells. Actin was used as an internal control. (D) Plectin-1 was also highly expressed in the cell lines. GAPDH was used as an internal control.

### 3.3 *In vitro* and *in vivo* toxicity of Gd-Cy7-PTP/RGD

Probe toxicity testing is a critical prerequisite to biomedical applications. The possible cytotoxicity of both Gd-Cy7-PTP/RGD and its free monomers towards normal and PC cells was evaluated (Fig. S6). Cell viability of Panc1 (PC cells, ITGB4 and plectin-1 dual over-expressed), T3M4 (PC cells, moderate expressed), and HDPE6-C7 (normal human pancreatic ductal cell, rarely expressed) after incubation with Gd-Cy7-PTP/RGD, Gd, and free Cy7 (at concentrations of 0, 30, 60, 90, 120, and 150  $\mu\text{g/mL}$ ) for 48 h was determined by MTT tests. Significant cytotoxicity toward Panc1 and T3M4 cells was observed at probe concentrations as high as 90  $\mu\text{g/mL}$ , which far surpassed those used in the *in vitro* and *in vivo* experiments. No significant

cytotoxicity toward HPDE6-C7 cells was found at any probe concentrations, even up to 150  $\mu\text{g/mL}$ . All cell lines retained 86% viability at the tested concentrations. In addition, healthy mice were intravenously injected with a Gd/Cy7 complex (60  $\mu\text{g/mL}$ ) for *in vivo* toxicity testing. As shown in Fig. S7, there were no detectable acute (24 h post-injection) or chronic inflammatory responses (30 days post-injection) in the major organs, including the liver, spleen, kidney, pancreas, and muscle. These suggest that the Gd/Cy7 complex is stable and safe at test doses.

### 3.4 *In vitro* specific binding affinity of bi-peptides

After the safety of the bispecific probe was demonstrated *in vitro* and *in vivo*, cell target binding was examined by cellular immunofluorescence and flow cytometry and ELISA.

Firstly, human pancreatic cancer panc1 cells, mouse L929 fibroblast cells, human HUVEC cells and human normal pancreatic duct epithelial cells as HPDE6-C7 cells were incubated with PTP-labeled AF647 and RGD-labeled AF488 in Fig.S8. On the one hand, it was clear whether there were differences in the affinity of the probes for different types of cells, and on the other hand, the co-localization value of the two peptides probe. Overlap scatterplots and Mander's coefficient for overlap of human pancreatic cancer panc1 cells, mouse L929 fibroblast cells, human HUVEC cells and human normal pancreatic duct epithelial cells as HPDE6-C7 cells was 0.83, 0.47, 0.34, 0.25, respectively, using *Image-proplus* 6.0 software.

The binding affinity of single peptides was demonstrated, is shown in Fig. S9A, and is quantitatively analyzed in Fig. S9B. AF647-labeled RGD and AF488-labeled PTP co-incubated with Panc1 cells revealed much stronger fluorescent intensity outside nuclei than did the blocking control pre-incubated with plectin-1/ITGB4 McAb for 4 h. Additionally, fluorescence intensity differences were clearly observed between single staining and blocking. Mean fluorescence intensity was quantitatively analyzed using *Image J* 2X, and significant differences between fluorescence values were observed in the AF647-labeled RGD and AF488-labeled PTP groups via single blocking; the differences were even more clear in the bi-peptide complex-blocking

group. Hence, single peptides had good binding affinity to Panc1 cells, and their combined application was targeted Panc1 cells more strongly. Notably, fluorescence visualization and quantitation of each single peptide demonstrated the above results. As shown in Fig. S9C, so many fluorescent signals distributed on the same line were found with the fluorescence colocalization function of *Image J 2X*, meaning that the single peptides were colocalized in Panc1 cells.

Secondly, to test the high affinity of FITC-labeled bi-peptide complexes to PC cells, fluorescence microscopy and flow cytometry were performed in Panc1 cells (plectin-1/ITGB4, dual overexpressed) and HPDE6-C7 cells (rarely expressed). Target binding *in vitro* was qualitatively and quantitatively evaluated. FITC-labeled bi-peptide complexes were used to stain Panc1 cells (positive cells) and free FITC was used as a nonspecific control. HPDE6-C7 cells were incubated with the bispecific probe as a negative control. As shown in Fig. 4A and 4B, Panc1 cells incubated with FITC-labeled bi-peptide complexes displayed stronger fluorescence intensity, signifying that the bi-peptides probe had higher targeting affinity to Panc1 cells than to HPDE6-C7 cells. Mean fluorescence intensity surrounding Panc1 cells was significantly higher than that surrounding HPDE6-C7 cells in Fig. 4E.

The results of flow cytometry were consistent with those of confocal imaging. Fluorescent cells were chosen as shown in Fig. S10. Targeting affinity towards Panc1 and HPDE6-C7 cells was assessed by fluorescence flow cytometry, and the results are shown in Fig. 4C and D, respectively. With increasing concentrations of FITC-labeled bi-peptide complexes, apparent fluorescent shifts were shown, and the fluorescence intensity of the probe significantly increased. However, no evident change in fluorescence intensity was observed in either the HPDE6-C7 cells (negative control) or the free FITC group (nonspecific control). Quantification by flow cytometry is shown in Fig. 4F and G; as FITC concentration increased, fluorescence intensity of FITC-labeled bi-peptide complexes reached  $9.125 \times 10^4$  and was nearly saturated at 2.0  $\mu\text{g/mL}$  of FITC.

However, the fluorescence intensity of Panc1 cells incubated with free FITC did not exceed  $2 \times 10^4$ . HPDE6-C7 cells, which lack binding sites for the PTP and RGD

peptides, exhibited relatively low fluorescence intensity when incubated with FITC-labeled bi-peptide complexes that did not exceed  $1.2 \times 10^4$ . Therefore, the bispecific probe was shown by confocal imaging and flow cytometry to effectively bind Panc1 cell depending on overexpression of plectin-1 and ITGB4. That is, by efficiently targeting both plectin-1 and ITGB4, the bispecific probe increased binding affinity to Panc1 cells but not to HPDE6-C7 cells.

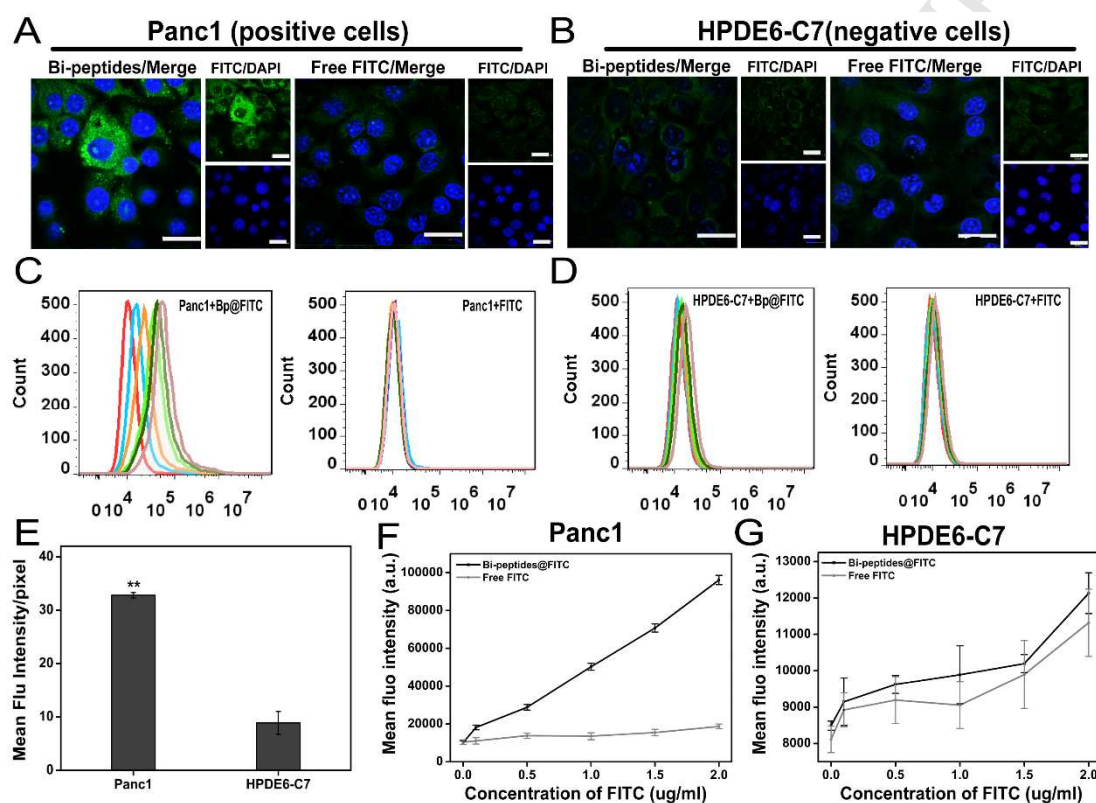


**Fig. 4. In vitro specific binding affinity of bi-peptides targeting.** (A) Panc1 cells (positive cells) were incubated with Gd/FITC complexes and free FITC for 4 h for cell fluorescent microscopy. (B) HPDE6-C7 cells (negative cells) were incubated with Gd/FITC complexes and free FITC for 4 h. Scale bar, 30  $\mu$ m. (C) Bispecific binding and nonspecific binding to Panc1 and (D) HPDE6-C7 cells were evaluated by flow cytometry. (E) Mean fluorescence intensity of Panc1 and HPDE6-C7 cells as analyzed by Image J 2X. (F) Mean fluorescence intensity of Panc1 and (G) HPDE6-C7 cells as analyzed by flow cytometry. \* $P < 0.05$ ; \*\*,  $P < 0.01$ ; \*\*\*,  $P < 0.001$ .

Lastly, the results of the cell binding study comparing the targeting ability of bi-peptide complexes and single peptides verified the advantage of our innovative design for bi-peptide targeting. As shown in Fig. 5A, compared with multiple blocking levels, FITC labeled bi-peptide complexes produced significantly stronger immunofluorescence staining of Panc1 cells, and were effectively blocked when the

cells were incubated with a saturating dose of anti-plectin-1, anti-ITGB4, or both antibodies before staining. Thus, the combination of the PTP and RGD peptides targeting PDAC increased binding efficiency.

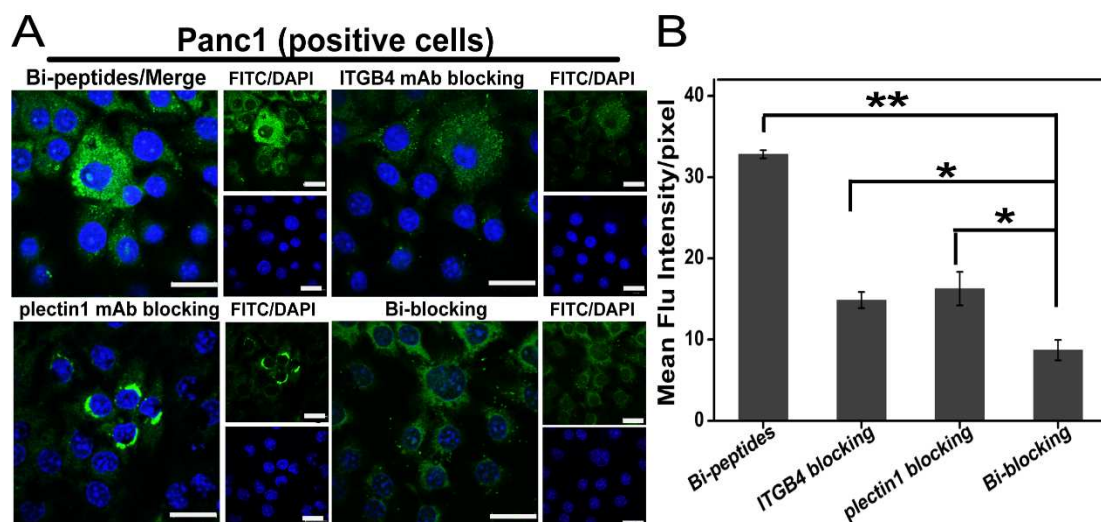


**Fig. 5. *In vitro* bispecific targeting.** (A) Fluorescent microscope images of Panc1 cells incubated with Gd/FITC complex and pre-incubated with an excess of either anti-ITGB4, anti-plectin-1, or both monoclonal antibodies. Scale bar, 30  $\mu$ m. (B) Mean fluorescence intensity of Panc1 cells was analyzed by *Image J* 2X. \* $P < 0.05$ ; \*\*,  $P < 0.01$ ; \*\*\*,  $P < 0.001$ .

For competition analysis, Plectin-1 and IGFB4 ELISA kits were used. Human Plectin-1 or IGFB4 first antibody, the corresponding IgG and Bi-peptide were added following bovine serum albumin (BSA) and cell homogenates incubation. Then perform the following steps in accordance with the ELISA kit. Both Plectin-1 antibody and bi-peptide can block Plectin-1 antigen in Panc1 and HPDE6-C7 cells' homogenates. IGFB4 antibody and bi-peptide also can block IGFB4 antigen in Panc1 and HPDE6-C7 cells' homogenates, as shown in Fig. S11.

Above all, confocal imaging and flow cytometry revealed evident enhancements in fluorescence intensity when Panc1 cells were incubated with FITC-labeled Gd-Cy7-PTP/RGD compared to that after multiple blockings. These results demonstrated that the bispecific PTP/RGD peptide targeted Panc1 cells with high affinity and excellent specificity. The enhanced targeting affinity toward PDAC and not normal pancreatic tissue is encouraging for its action *in vivo*.

### 3.5 *In vivo* microscopical imaging of bi-peptides targeting

Specific affinity was illustrated via the confocal images of pancreatic cancer cells. Subsequently, we wished to microscopically illuminate the specific affinity of bi-peptides to pancreatic cancer tissues. Hence, CFL imaging was used to further clarify the targeting affinity.

Nonspecific contrast agent fluorescein was used to outline the showed organizational structure of normal pancreatic and PDAC tissue, which can be seen at nearly single-cellular level in Fig. 6Aa and b. The obvious junction between normal pancreatic and PDAC tissue because of interstitial fibrosis due to carcinogenesis. And nonspecific fluorescein couldn't delineate cancerous tissue because of excessive fibrosis, as shown in Fig. 6Ac. Thus, CFL imaging with nonspecific fluorescein illustrated that interstitial fibrosis caused by pancreatic ductal epithelium carcinogenesis makes cancer and normal pancreatic tissue easy to distinguish. However, this ends with morphological changes.

To further explain the binding affinity of bispecific targeting, AF647-labeled PTP/RGD was used to target PDAC tissue. Fluorescein and AF647-labeled PTP/RGD were injected i.v. after 2 h and AF647-labeled PTP/RGD could outline the orthotopic PDAC to specifically target the PDAC tissues with high plectin1 and ITGB4 expression in Fig. 6B. And then, to confirm bispecific binding to PDAC with bi-peptides, bi-blocking tests were performed. Anti-plectin1 and anti-ITGB4 were injected 4 hours in advance for dual-blocking plectin1 and ITGB4 combination sites in order to verify binding specificity of bi-peptides. As shown in Fig. 6C, effective obturation function of plectin1/ITGB4 mAb made bi-peptides probe less in PDAC tissues and almost no localized in normal pancreatic tissues. Subsequently, CFL images with AF488-labeled RGD and AF647-labeled PTP illustrated how a single-peptide works on targeting to PDAC tissues in Fig. 6D.

*Ex vivo* fluorescence images of tumor tissue cryosections were scanned by 3D HISTECH and read by Pannoramic Viewer to further reveal the targeting localization of RGD and PTP to PDAC, as shown in Fig. 6E. Differential localization in cancerous tissue was demonstrated, indicating that the bi-peptide complex strengthened targeting affinity and amplified the fluorescence signal. AF647-labeled PTP diffused

throughout the tumor tissue, and most of the PTP probe was densely distributed at the tumor periphery, which may be because the peripheral tumor cells were more active than those in the center. However, AF488-labeled RGD accumulated at the tumor centers, suggesting that it widely bind to integrin family proteins, not only acting on ITGB4 overexpressed on the PDAC epithelium but also targeting tumor angiogenesis. Under greater magnification, AF488-labeled RGD and AF647-labeled PTP overlapped in tumor tissue, as shown in Fig. 6F k and I, more clearly explained that PTP targeting to tumor parenchyma tissue with high fluorescent level while RGD extensively targeting the entire tumor tissue, especially tumor vessels.

Using CFL imaging with fluorescence probes, the mechanism by which bi-peptides probe targets and localizes to PDAC was demonstrated, and probe distribution, signal intensity, and cellular morphology were examined. Bi-peptide complexes demonstrated facile targeting of plectin-1 and ITGB4 for the early detection critically needed in PDAC. Bi-peptide design of bi-peptides probe had higher PDAC targeting capability than did either single peptide.

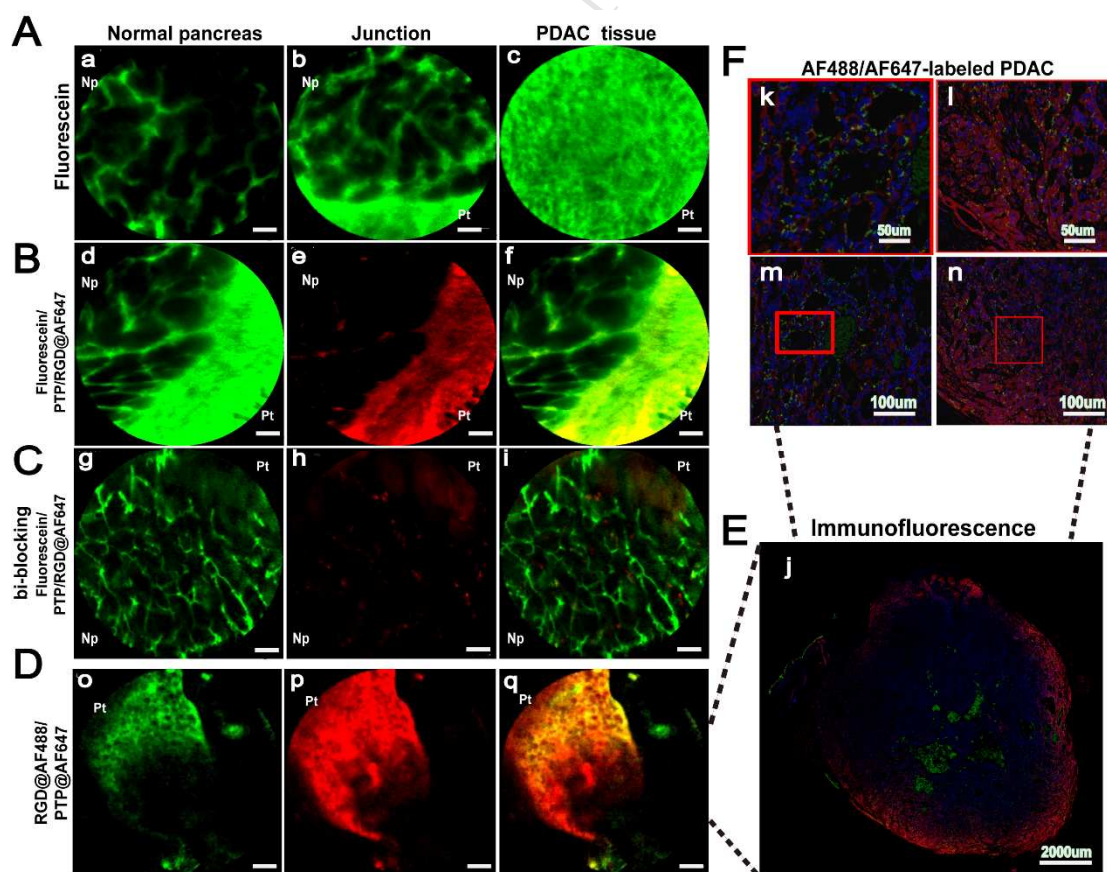


**Fig. 6. *In vivo* microscopical imaging of bi-peptides targeting.** (A) CFL imaging *in vivo* of fluorescein (green color) to outline organizational structure of normal pancreatic and PDAC tissue. Scale bar, 20  $\mu$ m. (B) CFL imaging of AF647-labeled PTP/RGD bispecific probes (red color) and nonspecific fluorescein (green color) was performed after 2 h post-injection i.v. Scale bar, 20  $\mu$ m. (C) CFL imaging of AF647-labeled PTP/RGD bispecific probes (red color) and nonspecific fluorescein (green color) was performed beforehand plectin1 and ITGB4 binding sites were enclosed by anti-plectin1 and anti-ITGB4 mAb for 4 h in advance for dual-blocking. (D) CFL imaging of RGD/AF488 (green color) and PTP/AF647 (red color) was performed for further explanation the binding affinity of single peptide. Scale bar, 20  $\mu$ m. (E) Tumor tissues were resected 4 h after injection of RGD/AF488 and PTP/AF647. Cryosections were scanned by 3D HISTECH at 407 nm (blue color), 488 nm (green color), and 660 nm (red color) for tissue visualization by immunofluorescence. AF488-labeled RGD is shown in green and AF647-labeled PTP was shown in red. (F) AF488-labeled RGD (m, k) and AF647-labeled PTP (n, l) were illustrated in details for further illustration of single peptide distribution difference.

### 3.6 *In vivo* bio-distribution and dual-modality imaging of Gd-Cy7-PTP/RGD

Bispecific targeting and bio-distribution *in vivo* were explored by noninvasive NIRF/MRI imaging, which reflected the tumor-targeting characteristic of the Gd/Cy7 complex. Stable fluorescence of the probe at about 750 nm (Fig. 2A) enabled non-invasive monitoring and quantitative evaluating of its bio-distribution *in vivo*. Hence, the mice bearing subcutaneous Panc1 tumors were intravenously injected with Gd-Cy7-PTP/RGD (150  $\mu$ L/mouse, 400  $\mu$ g/mL) to examine its targeting and bio-distribution behavior *in vivo*. Bio-distribution was observed by fluorescence imaging. NIRF images of mice injected with Gd-Cy7-PTP/RGD without blocking, with plectin-1 McAb blocking, with ITGB4 McAb blocking, and with free Cy7 are presented in Fig. 7Aa–d.

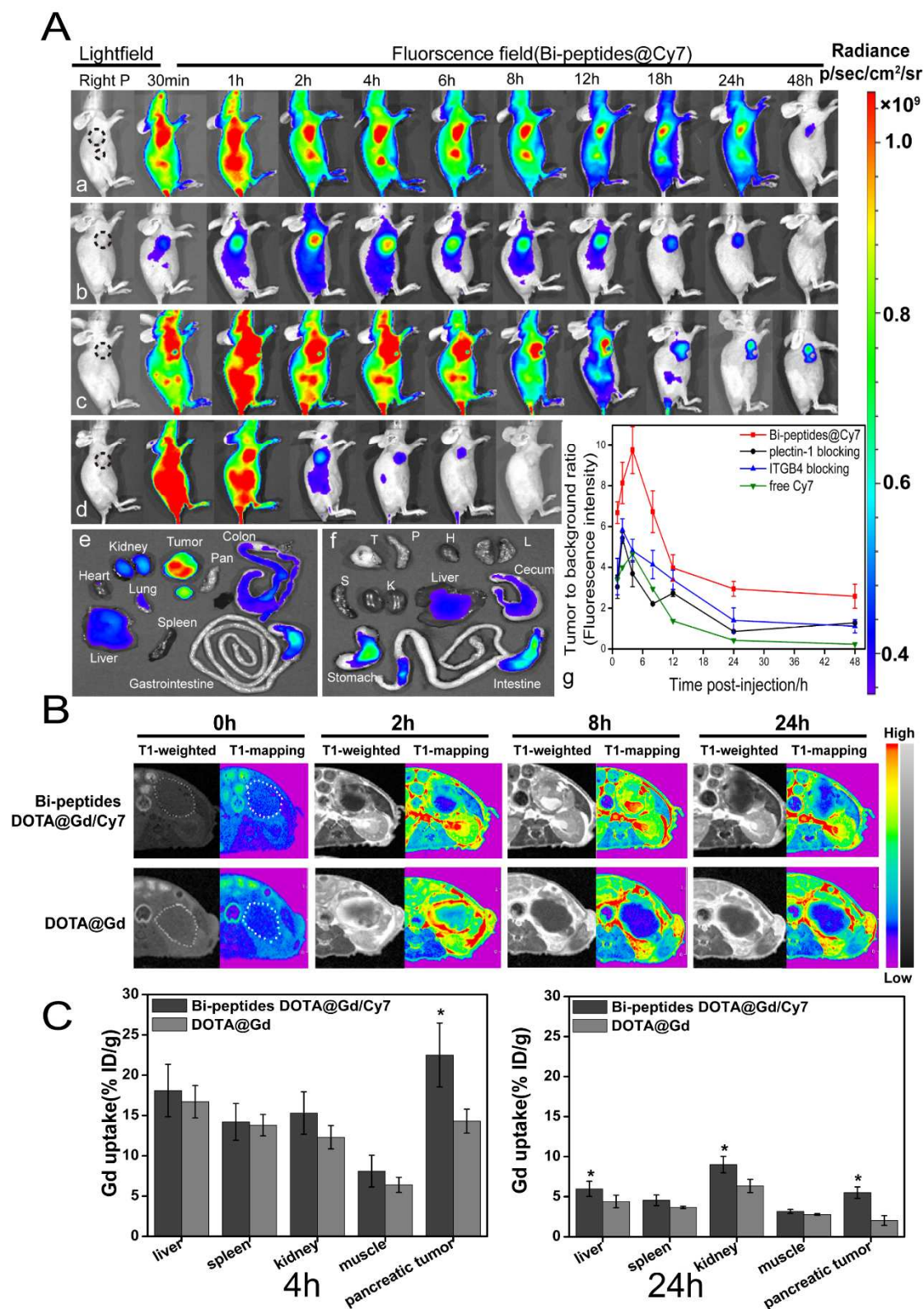


**Fig. 7. In vivo bio-distribution and dual-modality imaging of Gd-Cy7-PTP/RGD.**  
 (A) *In vivo* fluorescence images of the bispecific probe with and without multiple blockings in mice bearing Panc1 tumors at different time points post-injection. a: Mice injected with bispecific probe; b: Mice pre-injected with an excess of plectin-1 McAb; c: ITGB4 McAb blocking; d: free Cy7 injected; e: *ex vivo* fluorescence images of resected tumor and major organs from

probe-injected mice 24 h after injection; f: *ex vivo* organs from mice injected with free Cy7; g: TBR distribution. (B) MRI images of Gd-Cy7-PTP/RGD and Gd in mice bearing Panc1 tumors at different time points after injection. (C) Gd bio-distribution in tumor and major organs as visualized by ICP-OES.  $P < 0.05$ ; \*\*,  $P < 0.01$ ; \*\*\*,  $P < 0.001$ .

Considerable fluorescence changes were observed near tumors and the TBR (tumor background ratio) distinctly changed 30 min after injection. Fluorescence intensity in the tumors gradually increased within 4 h of injection, and TBR reached a 9.46 maximum (Fig. 7Ag), indicating that the probe continually accumulated near the tumors. Within 24 h of injection, strong fluorescence intensity remained at the tumor sites in the bispecific probe group (Fig. 7Aa), but no fluorescence signal was observed in the free Cy7 group 8 h after injection (Fig. 7Ad), demonstrating the better retention and longer cycle time of the bispecific probe than of free Cy7 near the tumors. Plectin-1 and ITGB4 blocking produced better fluorescence intensity and longer cycle times than did free Cy7; however, they produced lower fluorescence and shorter cycle times than did staining with the bispecific probe, as shown in Fig. 7Ag. This suggests that the bispecific probe has targeting ability than do single peptides, which necessary for effective molecular imaging, good TBR, and long-term cycle time of molecular probes [30]. As shown in Fig. 7Ae, *ex vivo* fluorescence images of major organs from mice injected with the bispecific probe were obtained 24 h after injection. Considerable fluorescence was found in resected tumors and weak residual signals were found in some organs, including the liver, kidneys, and intestines. However, almost no free Cy7 signal was detected in tumors, while weak signals were still present in the major organs, as shown in Fig. 7Af. At 4, 8, 24, and 48 h post-injection, the fluorescence intensity in tumors and major organs was examined using *ex vivo* images shown in Fig. S12. Fluorescence intensity at tumor sites was obviously higher than that in other tissues at all observed time points, further explaining the distribution of the bispecific probe in tumors and in major organs.

The excellent accumulation of the bispecific probe in tumors is based on efficient binding and prolonged cycle time. Good TBR depended not only on high tumor signal but also on low background signals, which was why a small molecular probe was chosen for targeting PDAC. In terms of metabolic characteristics, small molecular

probes have some incomparable advantages. They are characterized by easy permeability and take advantage of electron paramagnetic resonance (EPR) effects as well as convenient excretion based on their small molecular weights and sizes [35, 36]. Easy permeability and EPR effects contributed to the high probe concentration and fluorescence intensity at the tumor sites in this study. Further, because of their small molecular sizes, the probe had no immunogenicity, and easily escaped the RES (reticuloendothelial system absorption) monitor, resulting in negligible uptake by the liver and spleen and decreasing background noise. The probe did show increased kidney uptake, which may have been associated with renal excretion.

According to our design, Gd-Cy7-PTP/RGD was expected to improve *in vivo* tumor fluorescence and MR imaging. Increasing the Gd(III) concentration near tumors was key to successful molecular MRI. Small molecular probes with MR modules make use of easy permeability and EPR effects to more effectively enhance Gd(III) concentration in tumor sites than do nanoparticles, which rely only on EPR effects. Both advantages are critical for imaging of dense malignancies, particularly in pancreatic cancer, which is characterized by extreme hypoperfusion, hypovascularity, and high interstitial pressure. Nevertheless, the targeting element and NIFR module increased the molecular weight and decreased the Gd(III) concentration of the probe. To cope with this problem, the design incorporated dual DOTAs chelated to two Gd(III)s to enhance  $T_1$ -weighted relaxation. *In vivo* MRI was performed at varying time points after injection of Gd-Cy7-PTP/RGD to demonstrate its performance using Gd as a control.

The results in Fig. 7B clearly demonstrate that the  $T_1$ -weighted signals in the axial position gradually changed in the tumors of mice bearing orthotopic human Panc1 cells treated with Gd-Cy7-PTP/RGD. Compared with fluorescent imaging, which supplies only two-dimensional information about probe metabolism, MRI tomography provides more valuable details.  $T_1$ -weighted signals gradually permeated from well-perfused peripheral to non-perfused central regions of the pancreatic tumors. Notably, brighter  $T_1$ -weighted signals and prolonged retention caused by probe accumulation gradually enhanced until 8 h post-injection. However, the

$T_1$ -weighted signals of Gd decreased at 4 h post-injection. To examine metabolism of the probe, Gd(III) retention was quantified in tumor sites, as shown in Fig. 7C. The tumor tissues were collected from the mice *in vivo* at different time intervals post-injection and solubilized with a lysis solution. The homogenized lysates were diluted and measured by ICP-OES to quantitatively determine the concentrations of Gd(III) in the tumor tissues. Higher concentrations were found in tumors than in major organs, including the liver, spleen, and kidney, consistently with the *in vivo* fluorescence results at 4 h post-injection. However, superior Gd(III) uptake emerged in the kidneys compared to that in tumors at 24 h post-injection, suggesting that renal excretion was the primary metabolic pathway for the probe. Absolute  $T_1$  and SNR (signal noise ratio) were determined at different times post-injection, as shown in Fig. S13. Absolute  $T_1$  was representative of  $R_1$  relaxation.  $R_1$  relaxation of the bispecific probe was obviously increased compared to that of Gd, and SNR of the probe was also evidently enhanced and prolonged. Thus, the higher Gd(III) concentration and longer blood cycle time of the bispecific probe contributed to the better  $T_1$ -weighted signals in tumor sites than those observed after injection of Gd alone.

### 3.7 NIRF-guided surgery for orthotopic pancreatic tumors

Fluorescence and MR imaging using Gd-Cy7-PTP/RGD were performed, and intraoperative NIRF guidance was demonstrated on mice bearing orthotopically growing Panc1-luc xenograft tumors. Bioluminescence (BLI) imaging of the orthotopic xenograft model showed remarkable fluorescence intensity and sizable volume 27 days after Panc1-luc cell implantation in the tails of normal pancreases. Bioluminescence tomography (BLT) imaging further accurately and three-dimensionally located the orthotopic xenografts in the left abdominal region, as shown in Fig. 8A. Under the guidance of NIRF imaging, the tumors were successfully and entirely removed by surgery, as shown in Fig. 8B and C. The removed tumor tissues were then subjected to histological analysis. H&E staining of the dissected tumors further confirmed that resection margins were negative, as shown in Fig. 8Da. Paraffin-embedded sections of the tumors were used to observe tumor heterogeneity

by immunohistochemical staining of PNCA (proliferating cell nuclear antigen). Nuclear staining was medium and dark brown, suggesting malignant proliferation and high heterogeneity according to the characteristics of pancreatic neoplasia, as shown in Fig. 8Dc. Cryosections were cut into 20  $\mu\text{m}$  slices for NIRF imaging by inverted fluorescence microscopy (800 nm). NIRF imaging revealed that most of the bispecific probe-positive area overexpressed human plectin-1 and ITGB4, as shown in Fig. 8e, and that strong NIR signals were found in the whole tumor region, demonstrating that Gd-Cy7-PTP/RGD had the capability to effectively trace the PDAC xenograft tumor.

While optical imaging has some limitations in deep tissue and image reconstruction and quantification, it can be easily adapted for intraoperative guidance. Excellent intraoperative guidance using Gd-Cy7-PTP/RGD was verified, and similar probes have great potential for clinical application. Highly specific NIRF probes could improve intraoperative location and evaluation of suspicious lesions during surgery and provide fast assessment of resection margins to avoid residual tumor tissue and relapse. Stirringly, similar approaches to indocyanine green fluorescence-guided surgery have already been successfully applied to detection of the chest sympathetic nerve in lung cancer and resection of sentinel lymph nodes in breast cancer [37, 38].

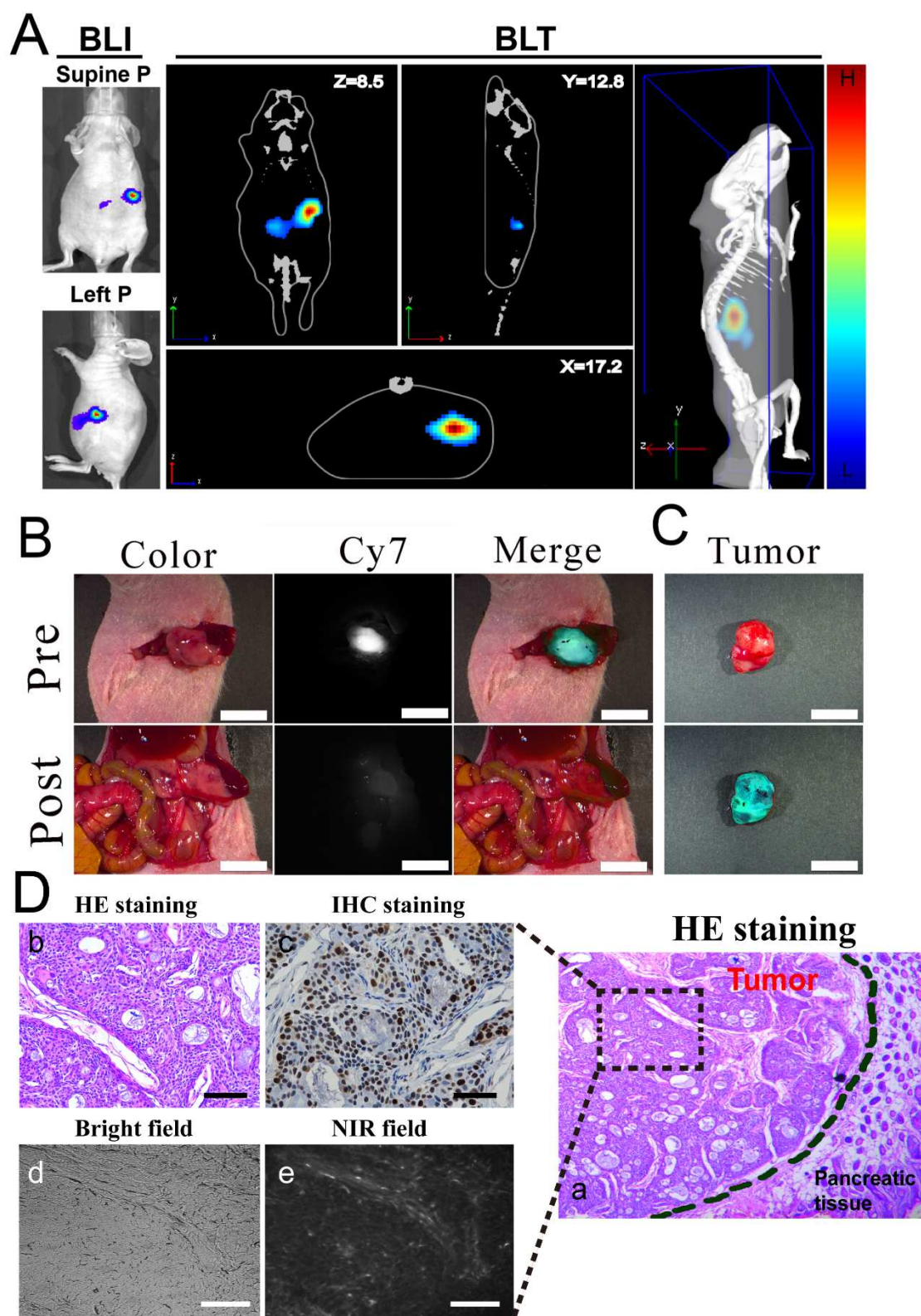


**Fig. 8. NIRF-guided surgery for orthotopic pancreatic tumors.** (A) BLI and BLT located pancreatic tumors. (B) NIRF imaging-guided intraoperative location and removal of orthotopic xenografts from mice bearing Panc1-luc tumors. Scale bar, 30  $\mu$ m. (C) The tumor was to be removed. (D) Histological analysis and NIRF imaging for surgery. a: H&E staining of resected tumor and partial normal pancreas; b: H&E staining of tumor tissue; c: immunohistochemical

staining of PCNA; d: cryosections imaged by inverted fluorescence bright-field and e: NIRF field microscopy (magnification: a, 40×; b–e, 200×).

#### 4. Conclusions

In summary, we have prepared a plectin/integrin-targeted bispecific molecular probe, Gd-Cy7-PTP/RGD, and applied it to MRI/NIRF dual-modality imaging-guided early PDAC diagnosis and surgical resection. The combination of PTP/RGD peptides greatly enhanced the specificity of probe and increased its binding efficiency to PDAC due to the close relationship of the peptides and their interaction in PDAC tissue. Moreover, the PTP and RGD simultaneously bound malignant epithelial cells and angiogenesis in tumor stroma to achieve a “multi-level” targeting effect when used together *in vitro* and *in vivo*. The excellent targeting effect lays the foundation for the early diagnosis and treatment of PDAC. Under the guidance of MRI/NIRF dual-modality imaging, more accurate surgical excision of PADC tumors has been successfully achieved in an orthotopic pancreatic cancer model. The bispecific molecular probe shows great promise for clinical application in PDAC diagnosis and guided surgical resection.

#### Supporting Information

Supporting Information is available from the Elsevier Online database or from the author.

#### Conflict of interest

The authors declare no competing financial interest.

#### Acknowledgements

Q. Wang and H. Yan contributed equally to this work. This work was financially supported by the National Natural Science Foundation of China under grant Nos.

81671757, 81527805, and 61671449; the National Key Research and Development Program of China under grant Nos. 2017YFA0205200, 2016YFA0201401, and 2106YFC0103702; and the CAMS Innovation Fund for Medical Sciences under grant No. 2016-I2M-1-001.

## References

- [1] R. Siegel, J. Ma, Z. Zou, A. Jemal. Cancer Statistics, 2014. *Ca-a Cancer Journal for Clinicians* 2014; 64: 9-29.
- [2] L. Zhu, C. Staley, D. Kooby, B. El-Rays, H. Mao, L. Yang. Current status of biomarker and targeted nanoparticle development: The precision oncology approach for pancreatic cancer therapy. *Cancer Lett* 2017; 388: 139-148.
- [3] R.L. Siegel, K.D. Miller, A. Jemal. Cancer Statistics, 2016. *Ca-a Cancer Journal for Clinicians* 2016; 66: 7-30.
- [4] S. Eser, M. Messer, P. Eser, A. von Werder, B. Seidler, M. Bajbouj, R. Vogelmann, A. Meining, J. von Burstin, H. Alguel, P. Pagel, A.E. Schnieke, I. Esposito, R.M. Schmid, G. Schneider, D. Saur. In vivo diagnosis of murine pancreatic intraepithelial neoplasia and early-stage pancreatic cancer by molecular imaging. *Proceedings of the National Academy of Sciences of the United States of America* 2011;108: 9945-9950.
- [5] B. Agarwal, A.M. Correa, L. Ho, Survival in pancreatic carcinoma based on tumor size, *Pancreas* 36(1) (2008) E15-E20.
- [6] S. Yachida, S. Jones, I. Bozic, T. Antal, R. Leary, B. Fu, M. Kamiyama, R.H. Hruban, J.R. Eshleman, M.A. Nowak, V.E. Velculescu, K.W. Kinzler, B. Vogelstein, C.A. Iacobuzio-Donahue, Distant metastasis occurs late during the genetic evolution of pancreatic cancer, *Nature* 467(7319) (2010) 1114-U126.
- [7] J. Dimastromatteo, T. Brentnall, K.A. Kelly, Imaging in pancreatic disease, *Nature Reviews Gastroenterology & Hepatology* 14(2) (2017) 97-109.
- [8] P. Cinar, M.A. Tempero, Monoclonal Antibodies and Other Targeted Therapies for Pancreatic Cancer, *Cancer Journal* 18(6) (2012) 653-664.
- [9] C. Sorio, A. Mafficini, F. Furlan, S. Barbi, A. Bonora, G. Brocco, F. Blasi, G. Talamini, C. Bassi, A. Scarpa, Elevated urinary levels of urokinase-type plasminogen activator receptor (uPAR) in pancreatic ductal adenocarcinoma identify a clinically high-risk group, *Bmc Cancer* 11 (2011).
- [10] H. Zhou, W. Qian, F.M. Uckun, L. Wang, Y.A. Wang, H. Chen, D. Kooby, Q. Yu, M. Lipowska, C.A. Staley, H. Mao, L. Yang, IGF1 Receptor Targeted Theranostic Nanoparticles for Targeted and Image-Guided Therapy of Pancreatic Cancer, *Acs Nano* 9(8) (2015) 7976-7991.
- [11] M.M. Yallapu, M.C. Ebeling, S. Khan, V. Sundram, N. Chauhan, B.K. Gupta, S.E. Puumala, M. Jaggi, S.C. Chauhan, Novel Curcumin-Loaded Magnetic Nanoparticles for Pancreatic Cancer Treatment, *Mol Cancer Ther* 12(8) (2013) 1471-1480.
- [12] M.A. Pysz, S.B. Machtaler, E.S. Seeley, J.J. Lee, T.A. Brentnall, J. Rosenberg, F. Tranquart, J.K. Willmann, Vascular Endothelial Growth Factor Receptor Type 2-targeted

- Contrast-enhanced US of Pancreatic Cancer Neovascularity in a Genetically Engineered Mouse Model: Potential for Earlier Detection, *Radiology* 274(3) (2015) 790-799.
- [13] C. Xu, M.B. Wallace, J. Yang, L. Jiang, Q. Zhai, Y. Zhang, C. Hong, Y. Chen, T.S. Frank, J.A. Stauffer, H.J. Asbun, M. Raimondo, T.A. Woodward, Z. Li, S. Guha, L. Zheng, M. Li, ZIP4 is a Novel Diagnostic and Prognostic Marker in Human Pancreatic Cancer: A Systemic Comparison Between EUS-FNA and Surgical Specimens, *Current Molecular Medicine* 14(3) (2014) 309-315.
- [14] J. Dimastromatteo, J.L. Houghton, J.S. Lewis, K.A. Kelly, Challenges of Pancreatic Cancer, *Cancer Journal* 21(3) (2015) 188-193.
- [15] S. Jones, X. Zhang, D.W. Parsons, J.C.-H. Lin, R.J. Leary, P. Angenendt, P. Mankoo, H. Carter, H. Kamiyama, A. Jimeno, S.-M. Hong, B. Fu, M.-T. Lin, E.S. Calhoun, M. Kamiyama, K. Walter, T. Nikolskaya, Y. Nikolsky, J. Hartigan, D.R. Smith, M. Hidalgo, S.D. Leach, A.P. Klein, E.M. Jaffee, M. Goggins, A. Maitra, C. Iacobuzio-Donahue, J.R. Eshleman, S.E. Kern, R.H. Hruban, R. Karchin, N. Papadopoulos, G. Parmigiani, B. Vogelstein, V.E. Velculescu, K.W. Kinzler, Core signaling pathways in human pancreatic cancers revealed by global genomic analyses, *Science* 321(5897) (2008) 1801-1806.
- [16] M. Hidalgo, Pancreatic Cancer, *New England Journal of Medicine* 362(17) (2010) 1605-1617.
- [17] A.J. Boyle, P.-J. Cao, D.W. Hedley, S.S. Sidhu, M.A. Winnik, R.M. Reilly, MicroPET/CT imaging of patient-derived pancreatic cancer xenografts implanted subcutaneously or orthotopically in NOD-scid mice using Cu-64-NOTA-panitumumab F(ab')(2) fragments, *Nuclear Medicine and Biology* 42(2) (2015) 71-77.
- [18] 108. US National Library of Medicine. ClinicalTrials.gov, <https://clinicaltrials.gov/ct2/show/NCT01962909>(2013).
- [19] S.J. Shin, J.A. Smith, G.A. Reznicek, S. Pan, R. Chen, T.A. Brentnall, G. Wiche, K.A. Kelly, Unexpected gain of function for the scaffolding protein plectin due to mislocalization in pancreatic cancer, *Proceedings of the National Academy of Sciences of the United States of America* 110(48) (2013) 19414-19419.
- [20] J. Niu, Z. Li, The roles of integrin alpha v beta 6 in cancer, *Cancer Lett* 403 (2017) 128-137.
- [21] M. Ueda, T. Fukushima, K. Ogawa, H. Kimura, M. Ono, T. Yamaguchi, Y. Ikehara, H. Saji, Synthesis and evaluation of a radioiodinated peptide probe targeting alpha v beta 6 integrin for the detection of pancreatic ductal adenocarcinoma, *Biochemical and Biophysical Research Communications* 445(3) (2014) 661-666.
- [22] Z. Li, P. Lin, C. Gao, C. Peng, S. Liu, H. Gao, B. Wang, J. Wang, J. Niu, W. Niu, Integrin beta 6 acts as an unfavorable prognostic indicator and promotes cellular malignant behaviors via ERK-ETS1 pathway in pancreatic ductal adenocarcinoma (PDAC), *Tumor Biology* 37(4) (2016) 5117-5131.
- [23] P.P. Adiseshaiah, R.M. Crist, S.S. Hook, S.E. McNeil, Nanomedicine strategies to overcome the pathophysiological barriers of pancreatic cancer, *Nat Rev Clin Oncol* 13(12) (2016) 750-765.
- [24] H.F. Dvorak, J.A. Nagy, J.T. Dvorak, A.M. Dvorak, IDENTIFICATION AND CHARACTERIZATION OF THE BLOOD-VESSELS OF SOLID TUMORS THAT ARE LEAKY TO CIRCULATING MACROMOLECULES, *American Journal of Pathology* 133(1) (1988) 95-109.

- [25] A.M. Dvorak, S. Kohn, E.S. Morgan, P. Fox, J.A. Nagy, H.F. Dvorak, The vesiculo-vacuolar organelle (VVO): A distinct endothelial cell structure that provides a transcellular pathway for macromolecular extravasation, *Journal of Leukocyte Biology* 59(1) (1996) 100-115.
- [26] S. Wilhelm, A.J. Tavares, Q. Dai, S. Ohta, J. Audet, H.F. Dvorak, W.C.W. Chan, Analysis of nanoparticle delivery to tumours, *Nature Reviews Materials* 1(5) (2016).
- [27] H. Yan, L. Zhao, W. Shang, Z. Liu, W. Xie, C. Qiang, Z. Xiong, R. Zhang, B. Li, X. Sun, F. Kang, General synthesis of high-performing magneto-conjugated polymer core-shell nanoparticles for multifunctional theranostics, *Nano Research* 10(2) (2017) 704-717.
- [28] H. Yan, W.T. Shang, X.D. Sun, L.Y. Zhao, J.Y. Wang, Z.Y. Xiong, J. Yuan, R.R. Zhang, Q.L. Huang, K. Wang, B.H. Li, J. Tian, F.Y. Kang, S.S. Feng, "All-in-One" Nanoparticles for Trimodality Imaging-Guided Intracellular Photo-magnetic Hyperthermia Therapy under Intravenous Administration, *Adv Funct Mater* 28(9) (2018).
- [29] X. Wu, S.M. Burden-Gulley, G.P. Yu, M. Tan, D. Lindner, S.M. Brady-Kalnay, Z.R. Lu, Synthesis and evaluation of a peptide targeted small molecular Gd-DOTA monoamide conjugate for MR molecular imaging of prostate cancer, *Bioconjug Chem* 23(8) (2012) 1548-56.
- [30] Z. Zhou, X. Wu, A. Kresak, M. Griswold, Z.R. Lu, Peptide targeted tripod macrocyclic Gd(III) chelates for cancer molecular MRI, *Biomaterials* 34(31) (2013) 7683-93.
- [31] H. Luo, R. Hernandez, H. Hong, S.A. Graves, Y. Yang, C.G. England, C.P. Theuer, R.J. Nickles, W. Cai, Noninvasive brain cancer imaging with a bispecific antibody fragment, generated via click chemistry, *Proc Natl Acad Sci U S A* 112(41) (2015) 12806-11.
- [32] Y. Jin, X. Ma, S. Zhang, H. Meng, M. Xu, X. Yang, W. Xu, J. Tian, A tantalum oxide-based core/shell nanoparticle for triple-modality image-guided chemo-thermal synergetic therapy of esophageal carcinoma, *Cancer Lett* 397 (2017) 61-71.
- [33] J. von Burstin, S. Eser, B. Seidler, A. Meining, M. Bajbouj, J. Mages, R. Lang, A.J. Kind, A.E. Schnieke, R.M. Schmid, G. Schneider, D. Saur, Highly sensitive detection of early-stage pancreatic cancer by multimodal near-infrared molecular imaging in living mice, *Int J Cancer* 123(9) (2008) 2138-47.
- [34] J. von Burstin, S. Eser, M.C. Paul, B. Seidler, M. Brandl, M. Messer, A. von Werder, A. Schmidt, J. Mages, P. Pagel, A. Schnieke, R.M. Schmid, G. Schneider, D. Saur, E-cadherin regulates metastasis of pancreatic cancer in vivo and is suppressed by a SNAIL/HDAC1/HDAC2 repressor complex, *Gastroenterology* 137(1) (2009) 361-71, 371 e1-5.
- [35] T. Maldiney, A. Bessiere, J. Seguin, E. Teston, S.K. Sharma, B. Viana, A.J. Bos, P. Dorenbos, M. Bessodes, D. Gourier, D. Scherman, C. Richard, The in vivo activation of persistent nanophosphors for optical imaging of vascularization, tumours and grafted cells, *Nat Mater* 13(4) (2014) 418-26.
- [36] Q. le Masne de Chermont, C. Chaneac, J. Seguin, F. Pelle, S. Maitrejean, J.P. Jolivet, D. Gourier, M. Bessodes, D. Scherman, Nanoprobes with near-infrared persistent luminescence for in vivo imaging, *Proc Natl Acad Sci U S A* 104(22) (2007) 9266-71.
- [37] K. He, J. Zhou, F. Yang, C. Chi, H. Li, Y. Mao, B. Hui, K. Wang, J. Tian, J. Wang, Near-infrared Intraoperative Imaging of Thoracic Sympathetic Nerves: From Preclinical Study to Clinical Trial, *Theranostics* 8(2) (2018) 304-313.
- [38] K.S. He, C.W. Chi, D.Q. Kou, W.H. Huang, J.D. Wu, Y.B. Wang, L.F. He, J.Z. Ye, Y.M. Mao,

G.J. Zhang, J.D. Wang, J. Tian, Comparison between the indocyanine green fluorescence and blue dye methods for sentinel lymph node biopsy using novel fluorescence image-guided resection equipment in different types of hospitals, Translational Research 178 (2016) 74-80.